Polar growth protein Wag31 undergoes changes in homo-oligomeric network topology, and has distinct functions at both cell poles and the septum

Neda Habibi Arejan [a], Parthvi Bharatkumar Patel [a], Samantha Y. Quintanilla [a], Arash Emami Saleh [b], and Cara Boutte [a*]

[a] Department of Biology, University of Texas Arlington, Arlington, Texas, USA

[b] Department of Civil Engineering, University of Texas at Arlington, Texas, USA

*Corresponding author, cara.boutte@uta.edu

Abstract

Mycobacterial cell elongation occurs at the cell poles; however, it is not clear how cell wall insertion is restricted to the pole and organized. Wag31 is a pole-localized cytoplasmic protein that is essential for polar growth, but its molecular function has not been described. Wag31 homo-oligomerizes in a network at the poles, but it is not known how the structure of this network affects Wag31 function. In this study we used a protein fragment complementation assay to identify Wag31 residues involved in homo-oligomeric interactions, and found that amino acids all along the length of the protein mediate these interactions. We then used both N-terminal and C-terminal splitGFP fusions to probe Wag31 network topology at different sites in the cell, and found that Wag31 C-terminal-C-terminal interactions predominate at the septa, while C-terminal-C-terminal and C-terminal-N-terminal interactions are found equally at the poles. This suggests the Wag31 network is formed through an ordered series of associations. We then dissected Wag31's functional roles by phenotyping a series of *wag31* alanine mutants; these data show that Wag31 has separate functions in not only new and old

pole elongation, but also inhibition of both septation and new pole elongation. This work establishes new functions for Wag31, and indicates that changes in Wag31 homo-oligomeric network topology may contribute to cell wall regulation in mycobacteria.

Importance:

Many bacteria restrict cell wall elongation to their cell poles, but it is not known how polar growth is affected on the molecular level. Wag31 is a protein that is required for this polar elongation. In this work, we show that Wag31 actually has at least four distinct functions in regulating the cell wall: it promotes elongation at both poles in different ways, and it can also inhibit cell wall metabolism at the new pole and the septum. In addition, we propose a new model for how Wag31 self-associates into a protein network. This work is important because it shows that a DivIVA homolog can have distinct functions depending on cell context. And, this work clarifies that Wag31 is doing several different things in the cell, and gives us genetic tools to disentangle its functions.

Keywords: mycobacterium, cell elongation, polar growth regulation, peptidoglycan, DivIVA, IMD, network topology

Introduction

To grow, bacteria need to expand in size by cutting the existing peptidoglycan cell wall and adding new material without disturbing its integrity. Peptidoglycan is critical for maintenance of cell shape, and made of sugar chains crosslinked by small peptides. Many rod shaped organisms perform this cell wall expansion all along the lateral walls

(1, 2). Mycobacteria, as well as many other Actinomycetes and some Alphaproteobacteria, restrict cell wall expansion to the cell poles (3, 4). Lateral cell wall expansion in bacteria like *C. crescentus, E. coli*, and *B. subtilis* is controlled MreB, which directs the movement of cell wall enzymes at the site of expansion (2, 5). In Mycobacteria, there are no clear functional homologs of MreB, though the DivIVA domain protein Wag31 is essential for polar elongation (6).

New bacterial cells have a new pole, which is the product of cell division, and an old pole which is inherited intact from the mother. In mycobacteria, the old pole elongates continuously, but there is a delay in initiation of elongation at the new pole (7) which results in asymmetric cells (7, 8) (9). Polar growth is partly regulated by the Intracellular Membrane Domain (IMD), a chemically distinct region of the plasma membrane. The IMD is localized largely to the sub polar regions in growing mycobacterial cells (10). Cell wall precursors are thought to be synthesized and flipped in the IMD region (11). GlfT2 and MurG are IMD-associated enzymes which synthesize precursors for the arabinogalactan and the peptidoglycan layers of the wall, respectively (10).

In this paper we dissect the function of Wag31 (AKA DivIVA, Rv2145c, MSMEG_4217), a mycobacterial homolog of DivIVA. DivIVA proteins are found in Firmicutes and Actinobacteria (Fig. S1). They typically localize to the poles and/or septum, and function to recruit and regulate other factors that have functions in cell division, chromosome segregation and cell wall synthesis (12–16).

In pole-growing *Corynebacterium glutamicum*, DivIVA is essential for polar growth and localizes to the poles (17). $DivIVA_{Cg}$ recruits the essential peptidoglycan synthesizing enzyme RodA to the pole (16) and interacts with PBP1 (13); these interactions are thought to help restrict peptidoglycan synthesis to the pole. In *Streptomyces coelicolor*, DivIVA is involved in polar hyphal growth. It is localized at the hyphal tips and is important for hyphal elongation and splitting(18–21), though remains unclear on the molecular level how DivIVA works.

Wag31 is essential for polar growth in mycobacteria (6, 22), is localized at the poles (23, 24) and at the septum just before division(25) . Wag31 helps with chromosome segregation by recruiting the chromosome segregation factor ParA to the poles (26). Wag31 is not required for cell wall metabolism, but it is needed to direct this metabolism to the pole (27). Both RodA and PBP1 in *Msmeg* are delocalized around the entire cell instead of restricted to the poles (27). Thus, *Msmeg* does not regulate polar cell wall synthesis by restricting its essential peptidoglycan transglycosylases to the poles. However, *Msmeg* does restrict synthesis of many cell wall precursor enzymes near the poles, through association with the IMD(10, 27). Depletion of Wag31 destabilizes the IMD (11).

DivIVA proteins are predicted to have coiled coils (23), and are known to form large oligomers (13, 17, 28), which associate the membrane at the cell poles (29, 30). However, the topology of these oligomers is not understood, and is likely to differ between species (Fig. S1). The N-terminal 60-65 amino acid of $DivIVA_{Bsub}$ / Wag31 has

been crystallized (29, 31). These structures both have two helices involved in a parallel coiled-coil dimer (Fig. 2C). The C-terminus of $DivIVA_{Bsub}$ is thought to form anti-parallel coiled-coils with the C-termini overlapping in a 4-helix bundle (29). The C-terminal region of Wag31 in *Mtb* has low similarity to that of $DivIVA_{Bsub}$, so its structure is unknown. Wag31 is predicted to have coiled coils at its C-terminal helix, and an unstructured loop in the middle (Fig. S1B), which the $DivIVA_{B.sub}$ protein lacks.

In this work we show that much of the Wag31 protein is involved in homo-oligomerization, and that the topology of the Wag31 network seems to develop over the course of the cell cycle. We also identify a series of point mutants of *wag31* that exhibit diverse phenotypes, and indicate that Wag31 has roles in inhibition of new pole elongation and septal inhibition, in addition to its established roles in promoting elongation at the new and old poles.

Results

Wag31 has multiple sites of homo-oligomerization

DivIVA homo-oligomerization has been partially characterized in *B. subtilis* (28, 29), and there are separate homo-oligomeric interaction sites on the N and C-terminus of the protein. Functional and sequence differences of mycobacterial Wag31 and $DivIVA_{Bsub}$ led us to ask which parts of $Wag31_{Mtb}$ are involved in homo-oligomerization (Fig. S1).

We used the Mycobacterial Protein Fragment Complementation two-hybrid assay (32) to test a series of $Wag31_{Mtb}$ alanine mutants fused to the mDHFR fragment 3, (mDHFR

116 F3), for interaction with wild-type $Wag31_{Mtb}$ fused to mDHFR F1,2 (Fig. 1A). Interaction
117 of the two Wag31 proteins will reconstitue the split mouse DHFR, yielding trimethoprim
118 resistance in *M. smegmatis.* Almost all of the tested alanine mutants of $Wag31_{Mtb}$ failed
119 to promote trimethoprim resistance, with the exception of eight residues at the very N-
120 terminus (Fig. 1, Table S1A). To determine if these mutant $Wag31_{Mtb}$ proteins are
121 stable, we performed western blots on the two-hybrid strains using α-F3-DHFR
122 antibodies (Fig. 1BC) and found that some of the mutants disrupted stability, but most
123 interrupted homo-oligomerization (Fig. 1D).
124
125 These data indicate that many residues involved in homo-oligomerization, thus any
126 single mutation must not completely prevent interaction as other interaction residues are
127 still intact. Since our western blotting shows that these constructs are stable, we
128 conclude that this assay does detect differences in protein associations, but that it has
129 limited dynamic range with Wag31 fusions. Our results indicate that there are likely sites
130 of $Wag31_{Mtb}$ homo-oligomerization beyond just the N and C-terminal interactions
131 described in *B. subtilis* (29). These multiple interaction sites should allow for a complex
132 protein network.
133
134 **Wag31 homo-oligomers have differing topology at different sites in the cell**
135 To test whether oligomers of Wag31 have different conformations at the poles and the
136 septa, we used splitGFP probes (Fig. 2A) (33). In this method, GFP1-10 (the first ten
137 beta-strands of superfolderGFP) was fused to either the N-terminus or C-terminus of
138 $wag31_{Msmeg}$, and GFP11(final beta strand) was fused to the C-terminus of $wag31_{Msmeg}$

139 (Fig. 2A). One strain, called here the NT-CT reporter, (GFP1-10-Wag31 and Wag31-
140 GFP11) will fluoresce when the N-terminus of one Wag31 is near the C-terminus of
141 another. The other strain, called the CT-CT reporter (Wag31-GFP1-10 and Wag31-
142 GFP11) will fluoresce when the C-terminus of two Wag31 are near each other (Fig. 2A).
143 We were unable to test an NT-NT reporter, as the GFP11-Wag31 construct seemed to
144 block polar localization. We performed controls to ensure that the observed signal is not
145 due to splitGFP self-assembly (Fig. S7).
146
147 When the fusion constructs were induced, both reporter strains exhibited similar polar
148 fluorescence, which indicates that Wag31 homo-oligomers have both CT-CT and NT-
149 CT interactions (Fig. 2BE). At the septum, the number of cells with septal Wag31 is
150 significantly more in the CT-CT reporter than the NT-CT strain. Because the septum is
151 the site where Wag31 first homo-oligomerizes (Santi *et al.*, 2013), our data suggest that
152 newly formed Wag31 structures are more likely to have CT-CT homo-oligomeric
153 interactions. Once the septa become poles, CT-CT and NT-CT interactions are
154 equivalent.
155
156 We chose a subset of *wag31* alanine mutants to test in this assay. We used the WT
157 Wag31 NT and CT fusions to GFP1-10, and fused the *wag31* D7A, K20A, L34A,
158 NQQR199-202, and F255A mutants to GFP11 to evaluate whether these mutations
159 alter the topology of Wag31 homo-oligomers. We found that L34A reporter strain
160 resulted in diffuse signal in both NT-CT and CT-CT constructs (Fig. 2B). This leucine
161 forms an apparent hydrophobic interaction with L2 of the other monomer in the crystal

162 structure of the N-terminus (34). The Wag31 L34A protein is largely functional (Fig. 3).
163 These splitGFP data imply that L34A may be required for an early step in homo-
164 oligomerization, and that this mutant protein does not compete well with the WT Wag31
165 proteins present in this merodiploid strain. SplitGFP data with the other mutants did not
166 show significant, reproducible differences from the wild-type reporters.
167
168 **Wag31 has separate roles in several steps of the cell cycle**
169 Depletion of Wag31 leads to arrest of polar elongation, loss of pole structure, (6, 35)
170 and delocalization of peptidoglycan and mycomembrane metabolism (22). To dissect
171 Wag31's functional roles in these processes, we profiled the phenotypes of *Msmeg*
172 strains with *wag31* WT replaced by the stable alanine mutants of *wag31*, using L5
173 allele swapping (36) (Fig. 1BC). We were unable to swap some of the mutants, thus P2,
174 T4, K15, and EQR 210-3 are essential (Fig S2C).
175
176 We phenotypically profiled the *wag31* allele swap strains (Fig 3A-I). Most of the mutants
177 at the N-terminus of Wag31 impair growth rate, while most mutants in the middle and C-
178 terminus of the protein do not (Fig. 3B, S2A). Microscopy experiments many of the
179 mutants are short and/ or wide (Fig. 3ABCDE, S2). Most of the $wag31_{Mtb}$ mutant strains
180 have higher HADA signal, which is a proxy for peptidoglycan metabolism, than $wag31_{Mtb}$
181 WT strain (Fig. S3A, S5, S6), possibly because of increased permeability. To compare
182 localized peptidoglycan between strains, we used relative intensity at the poles and
183 septa. HADA stains the old pole more brightly (37); throughout we assume that the
184 brighter pole is the old pole.

185 Most mutants had lower relative HADA signal than WT at the old pole, and none have
186 higher signal (Fig. 3F, S3B). At the new pole most mutants have the similar signal to
187 WT, but a few near the N-terminus are dimmer than WT, and a few near the C-terminus
188 are brighter than WT (Fig. 3F, S3C). This data indicates that mutants in Wag31 can
189 have different impacts on the peptidoglycan metabolism at the two cell poles. Septal
190 HADA intensity is increased in a few mutants (D7A, K20A, DER 185,7,8), while it is
191 decreased in others (Fig. S4B), suggesting that Wag31 regulates peptidoglycan
192 synthesis at the septa as well. We also observe that the septal placement is shifted
193 toward either pole in some of the mutants (Fig. S4C).
194
195 A variety of different phenotypes indicative of assorted functional roles for Wag31 were
196 apparent across all the mutants. We chose five mutants that represented the range of
197 observed phenotypes for further study: D7A, K20A, L34A, NQQR199-202AAAA, and
198 F255A.
199
200 **Wag31 is involved in septal inhibition via glutamate 7**
201 As the first eight residues of Wag31 are not required for homo-oligomerization (Fig. 1).
202 We chose one mutant in this region for further study, D7A. The *wag31* D7A strain grows
203 slowly, and the cells are short and wide (Fig. 3BCD). There is a slight decrease in
204 HADA intensity, compared to WT, at both poles (Fig. 3F), but HADA intensity is
205 significantly increased at the septa (Fig. 3G).
206

To determine whether HADA staining at the poles is indicative of polar elongation or peptidoglycan remodeling(37), we performed pulse-chase-pulse staining with two colors of fluorescent D-amino acids. We stained first with HADA, then outgrew the cells without stain for 1.5 hours, then stained with the green fluorescent D-alanine NADA, and measured the length of the poles that are green and not blue (Fig. 3H). Results from this experiment show that the *wag31* D7A strain elongates more than the WT at the old pole, and elongation at the new pole is similar to WT (Fig. 3I).

Our data show that the *wag31* D7A mutant is not defective for elongation (Fig. 3I); however, the cell length is substantially decreased (Fig. 3C), suggesting that division activated at shorter cell lengths. The higher septal HADA staining (Fig. 3G, S4B) suggests that there is more peptidoglycan metabolism at the septum than in WT cells. This cell division may sometimes be too early, which could lead to the unusual number of ghosts in the *wag31* D7A phase images (Fig. 3A). These data suggest that Wag31 is involved in inhibition of septation through D7. As D7A is not involved in homo-oligomerization (Fig. 1), the effects of this mutation could be due to an inability to interact with other proteins or the cell membrane. We localized Wag31 D7A-GFPmut3 in a merodiploid strain and find that it localizes like the Wag31 WT-GFPmut3 at the poles and septum (Fig. 4).

Wag31 regulates polar elongation through N-terminal residue K20

The N-terminus of Wag31 is highly conserved (Fig. S1). This part of the protein dimerizes and has been structurally characterized (29, 34). In *Bacillus subtilis*, F17 is

230 involved in interaction with the membrane at the cell pole (29). In *Msmeg*, K20 is
231 equivalent to F17 in DivIVA$_{Bsub}$.
232
233 Our microscopy data shows that the *wag31* K20A mutant has decreased HADA staining
234 compared to WT at the old pole, but equivalent staining at the new pole (Fig. 3F). To
235 determine whether the HADA staining difference represents a difference in elongation,
236 we performed the pulse-chase-pulse experiment (Fig. 3H). The results show that the
237 *Wag31* K20A mutant elongates ~.26 mm less than the WT at the old pole, and ~.14 mm
238 less at the new pole (Fig. 3FHI). The defect in *wag31* K20A elongation (22% less) is
239 similar to the defect in cell length (18%), indicating that this mutant is defective in
240 elongation, especially at the old pole. The *wag31* K20A strain has similar septal
241 intensity as the WT (Fig 3G), implying that peptidoglycan metabolism there is
242 comparable; however, the septal location is shifted slightly toward the old pole (Fig.
243 S4C), which could be explained because the old pole is elongating more slowly.
244
245 To determine if K20 is involved in membrane association, we localized K20A-GFPmut3
246 in a merodiploid strain, because the allele swaps were not viable. The Wag31 first
247 associates with the membrane at the septum. Localization of Wag31-GFPmut3 to the
248 septum reflects its interaction with the membrane, whereas localization at the poles
249 reflects interaction with other Wag31 proteins. The Wag31 K20A-GFPmut3 protein does
250 not show a defect in polar localization indicating that K20 residue alone is not necessary
251 for polar localization. But it is defective in septal localization (Fig. 4BCD), indicating that
252 the Wag31 K20A mutant may be slightly impaired in its ability to adhere to the polar

membranes. Residue K20 promotes Wag31 homo-oligomerization (Fig. 1ACD). The polar growth phenotypes in the *wag31* K20A mutant could be due to defects in an unknown hetero-oligomeric interaction, or defects in the structure of the homo-oligomeric network which could affect membrane structure or dynamics at the pole, or affect the activity or localization of other proteins.

Wag31 regulates new pole elongation through L34

We found that the *wag31* L34A mutant also has a defect in polar elongation. The *wag31* L34A mutant has decreased HADA staining at both poles, the old pole staining is 1.5% less, and the new pole is ~11% less than the WT (Fig. 3F). The old pole of the *wag31* L34A strain elongates the same amount as the WT strain, but the new pole has ~24% less elongation (Fig. 3I). In the population of *wag31* L34A mutants that we characterized, ~65% had no observable elongation at the new pole, while only 11% of cells in the *wag31* WT population had no new pole elongation in the 1.5 hour assay. Thus, it appears that the Wag31 L34 residue contributes to both initiation and extension of the new pole. The short cell length and slow growth rate (Fig. 3ABC) are likely due to this defect in new pole elongation, as we did not observe defects in the intensity or location of septa (Fig. 3G, S4C). We localized the Wag31 L34A-GFPmut3 in a merodiploid, and it does not have defects in polar localization. It is slightly dimmer than the Wag31 WT-GFPmut3 at the septum (Fig. 4D), which is the site of new pole construction.

Wag31 inhibits new pole initiation through F255

276 We made several alanine mutants in the C-terminus of Wag31, which is not part of the
277 conserved DivIVA domain (Fig. S1). We found that in the *wag31* F255A mutant, there is
278 increased intensity of HADA at the new pole, and less at the old pole (Fig.3F). The
279 pulse-chase-pulse experiment shows that the *wag31* F255A strain elongates ~47%
280 more than the WT at the new pole, while the old pole elongates 5% less compared to
281 the WT strain (Fig. 3I). There is no difference in polar and septal localization between
282 the Wag31 F255A-GFPmut3 and the Wag31 WT-GFPmut3 (Fig. 4). The HADA septal
283 intensity is similar in the *wag31* F255A mutant compared to the WT (Fig. 3G), while
284 septal location is shifted toward to the old pole, which could result from the increased
285 elongation activity at the new pole (Fig. S4C). The *wag31* F255A grows as fast as the
286 WT strain (Fig. 3B), and the cells are slightly shorter and thicker than the WT (Fig.
287 3CDE). The apparently increased elongation may be balanced by increased septation
288 to result in shorter cells. These data indicate that Wag31 has inhibitory role on
289 elongation of the new pole through its C-terminal residues (Fig. S3). So, Wag31 can
290 both promote and inhibit polar growth.
291
292 **Maintenance of polar integrity is controlled by NQQR199-202 residues**
293 Wag31 is necessary for rod shape (6, 22, 23). Forming a straight rod requires that new
294 cell wall material be added evenly around the circumference of the cell. Previous work
295 showed cell bending when Wag31-eGFP replaces native Wag31 (24), suggesting that
296 deforming the Wag31 network may lead to uneven cell wall insertion. We observed a
297 similar curved cell morphology in the *wag31* NQQR199-202AAAA mutant (Fig. 3A).
298 While the *wag31* NQQR199-202AAAA mutant has slightly decreased HADA intensity at

299 the old pole (Fig. 3F), pulse-chase-pulse staining shows that that elongation is similar to
300 the Wag31 WT at both poles (Fig. 3I). There are no differences in localization of Wag31
301 NQQR199-202AAAA-GFPmut3 and Wag31 WT-GFPmut3 (Fig. 4). The NQQR199-202
302 residues are toward the middle and involved in Wag31 homo-oligomerization (Fig. 1).
303 We propose that the Wag31 NQQR199-202AAAA mutation alters the structure of the
304 oligomeric network to cause cell wall insertion to be uneven around the circumference
305 of the cell, leading to slight polar bulging and curved poles (Fig. 3A).
306

307 **Wag31's effects on MurG and GlfT2 localization do not correlate with effects on**
308 **polar growth**

309 Recent work suggests that localization of the enzymes that synthesize cell wall
310 precursors to the subpolar Intracellular Membrane Domain (IMD) may be critical in
311 restricting elongation to the pole (10, 27). Depletion of Wag31 has been shown to
312 delocalize the IMD(11), though it is not known if Wag31 regulates the IMD, or if the IMD
313 localization is merely dependent on an intact cell pole.
314

315 To probe whether Wag31 regulates IMD structure, we localized both GlfT2-mcherry2B
316 and MurG-Venus in selected Wag31 alanine mutants. GlfT2 is the last galactan
317 cytoplasmic enzyme in arabinogalactan synthesis (38). GlfT2 associates with the IMD,
318 and localizes in the typical pattern of IMD-associated proteins (10). MurG is the final
319 cytoplasmic enzyme in peptidoglycan precursor synthesis, has a similar localization
320 pattern as GlfT2, (24) and is found in both cytoplasmic and IMD fractions (11).
321

322 Our microscopy data show that localization of GlfT2-mcherry2B is significantly
323 decreased at the old pole in the *wag31* K20A, D7A, L34A and F255A mutants
324 compared to the WT (Fig. 5ABC), while it was unchanged at the new pole (Fig 5ABD).
325 Localization of MurG-Venus is slightly decreased at the old pole in the *wag31* D7A,
326 L34A and NQQR199-202 mutants compared to the WT (Fig. 5E), and largely unaffected
327 at the new pole (Fig. 5F). Across the mutants tested, polar elongation (Fig. 3HI) does
328 not correlate either with GlfT2 or with MurG localization signals at the poles (Fig. 5).
329 These data suggest that Wag31 may regulate the localization of IMD proteins, probably
330 indirectly and largely at the old pole, but that this regulation does not directly control
331 polar elongation.
332
333 **Discussion**
334 Wag31's molecular function in regulating the cell wall has remained obscure. Homology
335 with other systems predicts that Wag31's would recruit and regulate cell wall enzymes
336 at the pole (12, 16). However, the heterooligomeric interactions that have been
337 described for Wag31 – AccA3 (24, 39) and FtsI (40) - do not connect to Wag31's role in
338 restricting cell wall metabolism to the poles. Additionally, these interactions may be
339 indirect (AccA3,) or only exist under certain stress conditions (FtsI). The other
340 interaction that Wag31 makes is with itself. Here, we sought to probe the assembly of
341 the homo-oligomeric network, and to dissect Wag31's function in regulating the cell wall
342 (Fig. 6).
343
344 **Predictions about Wag31 network structure**

The predicted structure of DivIVA in *B. subtilis* has only two alpha-helices which are thought to be arranged end-to-end, forming a chain (29). In Wag31 in mycobacteria, the predicted structure has three helices, and a 33 amino acid loop between the helices 2 and 3 (Fig 6C). We predict that the long loop will allow more flexibility in the topology of the network and would likely allow branching of the network as helices 1 and 2 of a monomer could interact with different monomers than helix 3 (*e.g.*, Fig 6C vs Fig. 6DE). Wag31 is predicted to form coiled coils at its helices through hydrophobic interfaces. The hydrophobicity map of the predicted Wag31 Alphafold2 structure (41) shows a hydrophobic interface that forms the coiled coil of the N-terminal region (helices 1 and 2) in the crystal structure. Helix 3 also has a stripe of hydrophobic residues, which is likely the site of a double or triple coiled coil (42)(Fig. S1B). Helix 3 in Wag31 might form either a parallel or anti-parallel coiled coil with the helix 3 in another monomer (Fig. 6CDE). A parallel coiled coil would bring the C-terminal of two monomers near each other, while the anti-parallel coiled coil might bring the N-terminus of one monomer near the C-terminus of another.

We made one leucine to alanine mutation in helix 2, and this disrupted homo-oligomerization in both the two-hybrid and split-GFP assays (Fig. 1,2). The inability of this Wag31 L34A mutant to interact with Wag31 WT in the split-GFP assay, where it is competing for interaction with WT protein, indicates that this L34 residue may be important for an initial dimerization event. We therefore propose that these hydrophobic coiled-coil interactions may be the first to form as Wag31 monomers associate.

368 We also tested how numerous charged and polar residues along the length of the
369 Wag31 protein affect homo-oligomerization (Fig. 1). We found that, with the exception a
370 few residues at the very N-terminus, all the residues we tested contributed to Wag31
371 homo-oligomerization in the sensitive two-hybrid assay. We propose that the charged
372 residues on the surface of the coiled-coil structure may mediate further salt-bridge
373 interactions that help to expand the network via stacking of coiled-coils.
374
375 We used splitGFP reporters to measure the relative proportion of CT-CT interactions,
376 and NT-CT interactions. The CT-CT signal might result from parallel coiled-coils forming
377 on helix 3, while the NT-CT signal could result from either anti-parallel coiled-coils at
378 helix 3, or from stacking of chains of coiled-coils through the proposed salt bridges (Fig.
379 6CDE). We found that at the septum, where new Wag31 first interacts with the
380 membrane, CT-CT interactions predominate. This supports the idea that parallel coiled
381 coils form from helix 3 of neighboring dimers, and that these interactions form early in
382 the construction of the network (Fig. 6E). We expect that Wag31, like DivIVA in close
383 relative *C. glutamicum* (30), will diffuse very little once incorporated into the network.
384 Thus, new coiled-coil Wag31 chains likely accumulate at the poles in layers, where CT-
385 CT and NT-CT interactions are evenly balanced (Fig. 2). It is likely that other proteins
386 interact with the Wag31 network and alter its topology and structure (30).
387
388 **Dissection of Wag31 functions**
389 Wag31 had previously been known to be essential for polar growth (6, 27). Here, we
390 phenotypically profiled alanine mutants of residues all along the length Wag31 and

391 found a variety of different phenotypes which indicate that Wag31 has several distinct
392 functions in cell growth (Fig. 6AB). We found that the *wag31* K20A mutant is specifically
393 more defective in old pole elongation while the *wag31* L34A mutant is specifically more
394 defective in new pole elongation (Fig. 3). These results indicate that Wag31 is doing
395 something different at the new and old poles. The structure of the Wag31 homo-
396 oligomeric network could be different at the two poles, and these mutations could
397 interfere with the network structure. Or, these mutations might interfere with interactions
398 of Wag31 with other proteins that regulate cell wall synthesis.
399
400 Our characterization of the *wag31* D7A mutant indicates that Wag31 is involved in
401 downregulating septation. Wag31 had previously been shown to localize to the cell
402 division site before septation (25), and overexpression of Wag31-GFP was shown to
403 inhibit and mis-localize septa (23). D7 is not required for homo-oligomerization, so it is
404 likely involved a hetero-oligomeric interaction. Wag31 interacts with the septal PBP FtsI
405 and regulates FtsI stability under oxidative stress through residues 46-48 (NSD) (40).
406 We tested a *wag31* Δ46-48 mutant, as per (40) and found it was destabilized (Fig. 1C).
407 We also made a *wag31* NSD46-48AAA mutant, and found that it had normal cell length
408 (Fig. S2), so those residues do not affect FtsI activity in log. phase. The Wag31 D7
409 residue could possibly form a separate interaction with FtsI, or other septal factors (43).
410
411 We found that the *wag31* F255A mutant had increased polar elongation at the new pole
412 (Fig. 3). This suggests that Wag31 has a role in inhibiting new pole elongation. The
413 slower elongation at the new pole is partly controlled by membrane protein LamA (8).

414 Our work suggests that either Wag31 works separately to inhibit new pole elongation, or
415 that LamA may interact with Wag31 through F255 and interfere with Wag31's promotion
416 of new pole elongation.
417
418 Most of the mutants we characterized show a defect in GlfT2-mcherry2B and MurG-
419 Venus localizations at the old pole, but not at the new pole. The localization of GlfT2
420 and MurG at the poles did not correlate with polar elongation defects (Fig. 3,5),
421 indicating that polar localization of the IMD proteins is not the only determinant of polar
422 growth. These data suggest that Wag31 is at best an indirect regulator of the IMD, and
423 that regulation of the IMD is likely not Wag31's essential function.
424
425 In this work, we describe a new model for the assembly of the Wag31 homo-oligomeric
426 network (Fig 6). Many questions remain about the structure of this network, but our work
427 indicates that there are likely numerous homo-oligomeric interfaces and that the
428 structure of the network likely develops as a septal site turns into a pole (Fig. 2). We
429 also define new roles for Wag31 in regulating both septation and the inhibition of the
430 new pole, and identify residues that have dominant roles in Wag31's different functions
431 (Fig 6).
432
433 **Materials and Methods**
434 **Bacterial strains and culture conditions**
435 All *Msmeg* strains were grown in liquid culture in 7H9 (BD, Sparks, MD) medium
436 supplemented with 0.2% glycerol, 0.05%Tween 80, and ADC (5g/L albumin, 2 g/L

437 dextrose, 0.85 g/L NaCl, 0.003 g/L catalase). For most experiments, *Msmeg* strains
438 were grown on LB Lennox plates. DH5a, TOP10, and XL1-Blue *E.coli* cells were used
439 for cloning. For *E. coli*, antibiotics concentrations were: kanamycin – 50 µg/ml;
440 hygromycin - 100 µg/ml; nourseothricin - 40 µg/ml. For *Msmeg,* antibiotic concentrations
441 were: kanamycin - 25 µg/ml; hygromycin - 50 µg/ml; nourseothricin – 20 µg/ml;
442 trimethoprim - 50 µg/ml.
443
444 **Growth curves**
445 Strains were grown to log. phase in 7H9 with appropriate antibiotics, then diluted to
446 OD600 = 0.1 without antibiotics in a 96 well plate. A Synergy Neo2 linear Multi-Mode
447 Reader was used to shake the plates continuously for 18 hours at 37°C, and read OD
448 every 15 min. To find the doubling time for each strain, the raw data were analyzed with
449 exponential growth equation model using GraphPad Prism (version 9.1.2).
450
451 **Strain construction**
452 To build the allele replacement strains, first $wag31_{Msm}$ under its native promotor was
453 cloned into a kanamycin-marked L5 integrating vector and transformed into *Msmeg*
454 mc^2155. Then, *wag31* at its native locus was replaced with hygromycin resistance
455 cassette by dsDNA recombineering (44). This cassette was oriented so the hygR
456 promoter drives expression of downstream genes in the operon. Deletion of *wag31* from
457 the genome was confirmed with PCR checks. $wag31_{Msm}$ at the L5 site was swapped
458 with $wag31_{Mtb}$ alleles in a nourseothricin-marked L5-integrating vector using L5-phage
459 site allelic exchange as described (36). The transformants were screened by antibiotic

460 resistance in order to confirm allele swap. Vectors containing *wag31*$_{Mtb}$ mutants were
461 created using PCR stitching. All vectors were made using Gibson cloning (45). All
462 strains, plasmids and primers used are listed in supplemental material part (Table S2A,
463 S2B, S2C).
464
465 **Mycobacterial protein fragment complementation (M-PFC) assay**
466 *Msmeg* strains carrying Mycobacterial protein fragment complementation (M-PFC)
467 assay vectors were grown to log. phase and struck on 7H11 agar (BD Difco™, Thermo
468 Fisher Scientific) with or without trimethoprim at 50 µg/ml as described (32). Plates were
469 incubated at 37°C for 4 days, and then photographed.
470
471 **Immunoblot analysis**
472 *Msmeg* strains carrying M-PFC vectors were grown to log. phase (OD600 = 0.5-0.7),
473 pelleted, and lysed by bead beating (Disruptor Beads 0.1mm from Disruptor Genie®,
474 Mini-Beadbeater-16, Biospect). Supernatants were separated by SDS-PAGE and
475 transferred onto polyvinylidene difluoride (PVDF) membranes (GE Healthcare) and
476 blocked with BSA for 1 hour. The blot was probed with a-C-terminal-DHFR rabbit
477 antibody (1 :1000 Sigma-Aldrich, D0942) and goat anti-rabbit IgG HRP-conjugated
478 secondary antibody (1:10,000, Thermo Fisher Scientific 31460) in PBST. a-Rpob was
479 used as loading control (10 :10000, Thermo Fisher Scientific, MA1-25425). All bands
480 were quantified using Fiji and normalized to the controls.
481
482 **Microscopy**

483 All microscopy was performed on three biological replicate cultures of each strain using
484 a Nikon Ti-2 widefield epifluorescence microscope with a Photometrics Prime 95B
485 camera and a Plan Apo 100x, 1.45-numerical-aperture (NA) lens objective. Cells were
486 taken from log. phase culture in 7H9 and immobilized on 1.5% agarose pads made with
487 Hdb media. To detect GFPmut3 and splitGFP signal, a filter cube with a 470/40nm
488 excitation filter, a 525/50nm emission filter and a 495nm dichroic mirror was used. To
489 detect mCherry2B signal, a filter cube with a 560/40nm excitation filter, a 630/70nm
490 emission filter and a 585nm dichroic mirror was used. To detect HADA, a filter cube with
491 a 350/50nm excitation filter, a 460/50nm emission filter, and a 400nm dichroic mirror
492 was used. Image analysis was performed using MicrobeJ (46) to make cell ROIs and
493 extract fluorescence data from them. Fluorescence intensity data from MicrobeJ was
494 further analyzed using bespoke MATLAB code (see supplement).
495

496 **SplitGFP probing of Wag31 homo-oligomerization topology**

497 The split superfolder GFP used was described in (33). GFP1-10 (beta-strands 1-10 of
498 superfolderGFP) was fused to both the N and C terminus of wild-type *wag31*$_{\text{Msmeg}}$ in L5
499 integrating vectors under a P750-tet promotor. GFP11(final beta strand) was fused to
500 the C-terminus of *wag31*$_{\text{Msmeg}}$ wild-type or mutant alleles or mcherry2B under a P750-
501 tet promoter in a Giles integrating vector. All strains were grown to log. phase (OD600 =
502 0.15-0.2) and induced with Anhydrotetracycline hydrochloride (ATc) for 15 minutes, then
503 stained with HADA and continued inducing for 15 min more, then washed with PBS
504 tween80, fixed with 1.6% paraformaldehyde for 10 min, then resuspended again in PBS
505 tween 80 before microscopy. HADA staining allows us to distinguish the poles, as it

506 stains the old pole more brightly (37). All microscopy images were analyzed with Fiji and
507 MicrobeJ. Unpaired T-test was used to calculate the P-values using GraphPad Prism.
508

509 **Cell staining**

510 Cultures were stained with 1 µg/mL HADA (R&D systems) for 15 minutes with rolling
511 and incubation at 37°C. Stained cultures were then pelleted and washed in 7H9 before
512 imaging. For the pulse-chase-pulse elongation test, cells after 15 minutes of HADA
513 staining were resuspended into 7H9 for 1.5 hours of rolling and incubation at 37°C, then
514 stained with 1 µg/mL NADA (R&D systems) for 2 minutes at room temperature, washed
515 and resuspended in 7H9 before imaging.
516

517 **Acknowledgements**

518 This work was supported by NIH grant R01AI148917 to CCB.
519

520 **References**

521 1. Zhao H, Patel V, Helmann JD, Dörr T. 2017. Don’t let sleeping dogmas lie: new
522 views of peptidoglycan synthesis and its regulation. Molecular Microbiology
523 106:847–860.

524 2. Egan AJF, Errington J, Vollmer W. 2020. Regulation of peptidoglycan synthesis
525 and remodelling. Nat Rev Microbiol 18:446–460.

526 3. Brown PJB, de Pedro MA, Kysela DT, Van der Henst C, Kim J, De Bolle X, Fuqua
527 C, Brun YV. 2012. Polar growth in the Alphaproteobacterial order Rhizobiales.
528 Proceedings of the National Academy of Sciences 109:1697–1701.

529 4. Baranowski C, Rego EH, Rubin EJ. 2019. The Dream of a Mycobacterium.
530 Microbiology Spectrum 7.

531 5. Hussain S, Wivagg CN, Szwedziak P, Wong F, Schaefer K, Izoré T, Renner LD,
532 Holmes MJ, Sun Y, Bisson-Filho AW, Walker S, Amir A, Löwe J, Garner EC. 2018.
533 MreB filaments align along greatest principal membrane curvature to orient cell wall
534 synthesis. eLife 7:e32471.

535 6. Kang C-M, Nyayapathy S, Lee J-Y, Suh J-W, Husson RN. 2008. Wag31, a
536 homologue of the cell division protein DivIVA, regulates growth, morphology and
537 polar cell wall synthesis in mycobacteria. Microbiology 154:725–735.

538 7. Hannebelle MTM, Ven JXY, Toniolo C, Eskandarian HA, Vuaridel-Thurre G,
539 McKinney JD, Fantner GE. 2020. A biphasic growth model for cell pole elongation
540 in mycobacteria. Nat Commun 11:452.

541 8. Rego EH, Audette RE, Rubin EJ. 2017. Deletion of a mycobacterial divisome factor
542 collapses single-cell phenotypic heterogeneity. Nature 546:153–157.

543 9. Joyce G, Williams KJ, Robb M, Noens E, Tizzano B, Shahrezaei V, Robertson BD.
544 2012. Cell Division Site Placement and Asymmetric Growth in Mycobacteria. PLOS
545 ONE 7:e44582.

546 10. Hayashi JM, Luo C-Y, Mayfield JA, Hsu T, Fukuda T, Walfield AL, Giffen SR,
547 Leszyk JD, Baer CE, Bennion OT, Madduri A, Shaffer SA, Aldridge BB, Sassetti
548 CM, Sandler SJ, Kinoshita T, Moody DB, Morita YS. 2016. Spatially distinct and
549 metabolically active membrane domain in mycobacteria. PNAS 113:5400–5405.

550 11. García-Heredia A, Kado T, Sein CE, Puffal J, Osman SH, Judd J, Gray TA, Morita
551 YS, Siegrist MS. 2021. Membrane-partitioned cell wall synthesis in mycobacteria.
552 eLife 10:e60263.

553 12. Marston AL, Errington J. 1999. Selection of the midcell division site in Bacillus
554 subtilis through MinD-dependent polar localization and activation of MinC.
555 Molecular Microbiology 33:84–96.

556 13. Valbuena N, Letek M, Ordóñez E, Ayala J, Daniel RA, Gil JA, Mateos LM. 2007.
557 Characterization of HMW-PBPs from the rod-shaped actinomycete
558 Corynebacterium glutamicum: peptidoglycan synthesis in cells lacking actin-like
559 cytoskeletal structures. Mol Microbiol 66:643–657.

560 14. van Baarle S, Celik IN, Kaval KG, Bramkamp M, Hamoen LW, Halbedel S. 2013.
561 Protein-Protein Interaction Domains of Bacillus subtilis DivIVA. Journal of
562 Bacteriology 195:1012–1021.

563 15. Eswaramoorthy P, Winter PW, Wawrzusin P, York AG, Shroff H, Ramamurthi KS.
564 2014. Asymmetric Division and Differential Gene Expression during a Bacterial
565 Developmental Program Requires DivIVA. PLoS Genetics 10:e1004526.

566 16. Sieger B, Bramkamp M. 2015. Interaction sites of DivIVA and RodA from
567 Corynebacterium glutamicum. Front Microbiol 5.

568 17. Letek M, Ordonez E, Vaquera J, Margolin W, Flardh K, Mateos LM, Gil JA. 2008.
569 DivIVA Is Required for Polar Growth in the MreB-Lacking Rod-Shaped

570 Actinomycete Corynebacterium glutamicum. Journal of Bacteriology 190:3283–
571 3292.

572 18. Flärdh K. 2003. Essential role of DivIVA in polar growth and morphogenesis in
573 Streptomyces coelicolor A3(2). Molecular Microbiology 49:1523–1536.

574 19. Hempel AM, Wang S -b., Letek M, Gil JA, Flardh K. 2008. Assemblies of DivIVA
575 Mark Sites for Hyphal Branching and Can Establish New Zones of Cell Wall
576 Growth in Streptomyces coelicolor. Journal of Bacteriology 190:7579–7583.

577 20. Hempel AM, Cantlay S, Molle V, Wang S-B, Naldrett MJ, Parker JL, Richards DM,
578 Jung Y-G, Buttner MJ, Flardh K. 2012. The Ser/Thr protein kinase AfsK regulates
579 polar growth and hyphal branching in the filamentous bacteria Streptomyces.
580 Proceedings of the National Academy of Sciences 109:E2371–E2379.

581 21. Passot FM, Cantlay S, Flärdh K. 2021. Protein phosphatase SppA regulates apical
582 growth and dephosphorylates cell polarity determinant DivIVA in Streptomyces
583 coelicolor. Mol Microbiol https://doi.org/10.1111/mmi.14856.

584 22. Melzer ES, Sein CE, Chambers JJ, Sloan Siegrist M. 2018. DivIVA concentrates
585 mycobacterial cell envelope assembly for initiation and stabilization of polar growth.
586 Cytoskeleton 75:498–507.

587 23. Nguyen L, Scherr N, Gatfield J, Walburger A, Pieters J, Thompson CJ. 2007.
588 Antigen 84, an Effector of Pleiomorphism in Mycobacterium smegmatis. Journal of
589 Bacteriology 189:7896–7910.

590 24. Meniche X, Otten R, Siegrist MS, Baer CE, Murphy KC, Bertozzi CR, Sassetti CM.
591 2014. Subpolar addition of new cell wall is directed by DivIVA in mycobacteria.
592 Proceedings of the National Academy of Sciences 111:E3243–E3251.

593 25. Santi I, Dhar N, Bousbaine D, Wakamoto Y, McKinney JD. 2013. Single-cell
594 dynamics of the chromosome replication and cell division cycles in mycobacteria.
595 Nat Commun 4:2470.

596 26. Pióro M, Małecki T, Portas M, Magierowska I, Trojanowski D, Sherratt D,
597 Zakrzewska-Czerwińska J, Ginda K, Jakimowicz D. 2018. Competition between
598 DivIVA and the nucleoid for ParA binding promotes segrosome separation and
599 modulates mycobacterial cell elongation. Molecular Microbiology
600 https://doi.org/10.1111/mmi.14149.

601 27. Melzer ES, Kado T, García-Heredia A, Gupta KR, Meniche X, Morita YS, Sassetti
602 CM, Rego EH, Siegrist MS. 2021. Cell wall damage reveals spatial flexibility in
603 peptidoglycan synthesis and a non-redundant role for RodA in mycobacteria.
604 preprint. Microbiology.

605 28. Stahlberg H, Kutejová E, Muchová K, Gregorini M, Lustig A, Müller SA, Olivieri V,
606 Engel A, Wilkinson AJ, Barák I. 2004. Oligomeric structure of the Bacillus subtilis
607 cell division protein DivIVA determined by transmission electron microscopy:
608 Structure of DivIVA oligomer. Molecular Microbiology 52:1281–1290.

609 29. Oliva MA, Halbedel S, Freund SM, Dutow P, Leonard TA, Veprintsev DB, Hamoen
610 LW, Löwe J. 2010. Features critical for membrane binding revealed by DivIVA
611 crystal structure. The EMBO Journal 29:1988–2001.

612 30. Giacomelli G, Feddersen H, Peng F, Martins GB, Grafemeyer M, Meyer F, Mayer
613 B, Graumann PL, Bramkamp M. 2022. Subcellular Dynamics of a Conserved
614 Bacterial Polar Scaffold Protein. Genes 13:278.

615 31. Choukate K, Gupta A, Basu B, Virk K, Ganguli M, Chaudhuri B. 2020. Higher order
616 assembling of the mycobacterial polar growth factor DivIVA/Wag31. Journal of
617 Structural Biology 209:107429.

618 32. Singh A, Mai D, Kumar A, Steyn AJC. 2006. Dissecting virulence pathways of
619 Mycobacterium tuberculosis through protein-protein association. Proceedings of
620 the National Academy of Sciences 103:11346–11351.

621 33. Cabantous S, Terwilliger TC, Waldo GS. 2005. Protein tagging and detection with
622 engineered self-assembling fragments of green fluorescent protein. Nat Biotechnol
623 23:102–107.

624 34. Choukate K, Chaudhuri B. 2020. Structural basis of self-assembly in the lipid-
625 binding domain of mycobacterial polar growth factor Wag31. IUCrJ 7:767–776.

626 35. Jani C, Eoh H, Lee J, Hamasha K, Sahana M, Han J-S, Nyayapathy S, Lee J-Y,
627 Suh J-W, Lee S, Rehse SJ, Crick DC, Kang C-M. 2010. Regulation of Polar
628 Peptidoglycan Biosynthesis by Wag31 Phosphorylation in Mycobacteria. BMC
629 Microbiology 10:327.

630 36. Pashley CA, Parish T. 2003. Efficient switching of mycobacteriophage L5-based
631 integrating plasmids in *Mycobacterium tuberculosis*. FEMS Microbiology Letters
632 229:211–215.

633 37. Baranowski C, Welsh MA, Sham L-T, Eskandarian HA, Lim HC, Kieser KJ, Wagner
634 JC, McKinney JD, Fantner GE, Ioerger TR, Walker S, Bernhardt TG, Rubin EJ,
635 Rego EH. 2018. Maturing Mycobacterium smegmatis peptidoglycan requires non-
636 canonical crosslinks to maintain shape. eLife 7:e37516.

637 38. Beláňová M, Dianišková P, Brennan PJ, Completo GC, Rose NL, Lowary TL,
638 Mikušová K. 2008. Galactosyl Transferases in Mycobacterial Cell Wall Synthesis. J
639 Bacteriol 190:1141–1145.

640 39. Xu W, Zhang L, Mai J, Peng R, Yang E, Peng C, Wang H. 2014. The Wag31
641 protein interacts with AccA3 and coordinates cell wall lipid permeability and
642 lipophilic drug resistance in Mycobacterium smegmatis. Biochemical and
643 Biophysical Research Communications 448:255–260.

644 40. Mukherjee P, Sureka K, Datta P, Hossain T, Barik S, Das KP, Kundu M, Basu J.
645 2009. Novel role of Wag31 in protection of mycobacteria under oxidative stress.
646 Molecular Microbiology 73:103–119.

647 41. Jumper J, Evans R, Pritzel A, Green T, Figurnov M, Ronneberger O,
648 Tunyasuvunakool K, Bates R, Žídek A, Potapenko A, Bridgland A, Meyer C, Kohl
649 SAA, Ballard AJ, Cowie A, Romera-Paredes B, Nikolov S, Jain R, Adler J, Back T,
650 Petersen S, Reiman D, Clancy E, Zielinski M, Steinegger M, Pacholska M,

Berghammer T, Bodenstein S, Silver D, Vinyals O, Senior AW, Kavukcuoglu K, Kohli P, Hassabis D. 2021. Highly accurate protein structure prediction with AlphaFold. Nature https://doi.org/10.1038/s41586-021-03819-2.

42. Hagemans D, van Belzen IAEM, Morán Luengo T, Rüdiger SGD. 2015. A script to highlight hydrophobicity and charge on protein surfaces. Front Mol Biosci 2.

43. Wu KJ, Zhang J, Baranowski C, Leung V, Rego EH, Morita YS, Rubin EJ, Boutte CC. 2018. Characterization of Conserved and Novel Septal Factors in *Mycobacterium smegmatis*. Journal of Bacteriology 200:e00649-17, /jb/200/6/e00649-17.atom.

44. van Kessel JC, Hatfull GF. 2008. Mycobacterial Recombineering. Methods in Molecular Biology (Clifton, NJ) 435:203–215.

45. Gibson DG, Young L, Chuang R-Y, Venter JC, Hutchison CA, Smith HO. 2009. Enzymatic assembly of DNA molecules up to several hundred kilobases. Nat Methods 6:343–345.

46. Ducret A, Quardokus EM, Brun YV. 2016. MicrobeJ, a tool for high throughput bacterial cell detection and quantitative analysis. Nat Microbiol 1:16077.

47. Jumper J, Evans R, Pritzel A, Green T, Figurnov M, Ronneberger O, Tunyasuvunakool K, Bates R, Žídek A, Potapenko A, Bridgland A, Meyer C, Kohl SAA, Ballard AJ, Cowie A, Romera-Paredes B, Nikolov S, Jain R, Adler J, Back T, Petersen S, Reiman D, Clancy E, Zielinski M, Steinegger M, Pacholska M, Berghammer T, Bodenstein S, Silver D, Vinyals O, Senior AW, Kavukcuoglu K,

672 Kohli P, Hassabis D. 2021. Highly accurate protein structure prediction with
673 AlphaFold. Nature 596:583–589.

674 48. Choukate K, Chaudhuri B. 2020. Structural basis of self-assembly in the lipid-
675 binding domain of mycobacterial polar growth factor Wag31. IUCrJ 7:767–776.

A. Two-hybrid Assay

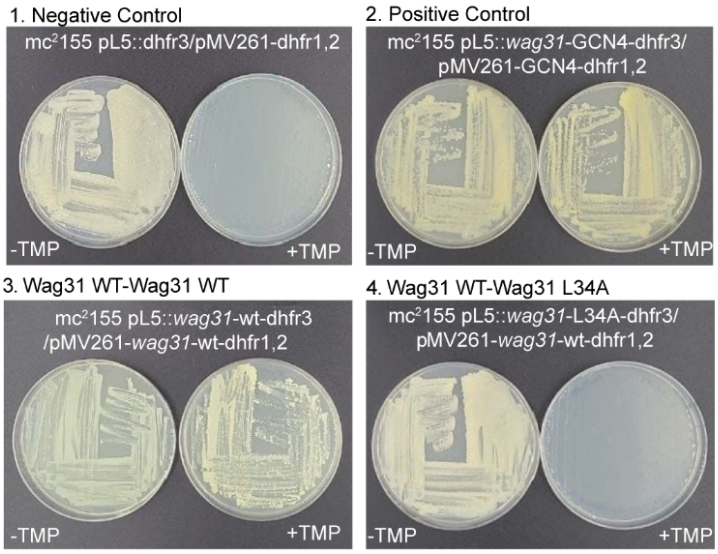

B. Stability of Wag31-DHFR3 fusions by western blot

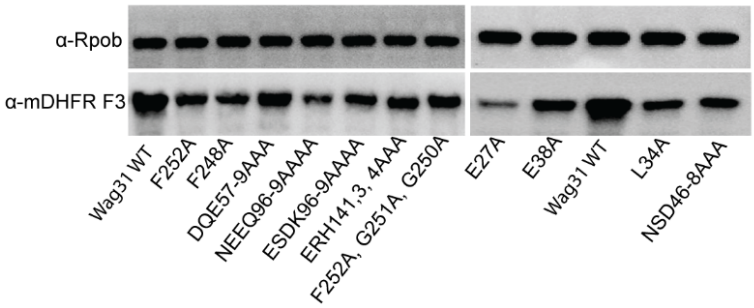

D. Residues involved in Wag31 homo-oligomerization

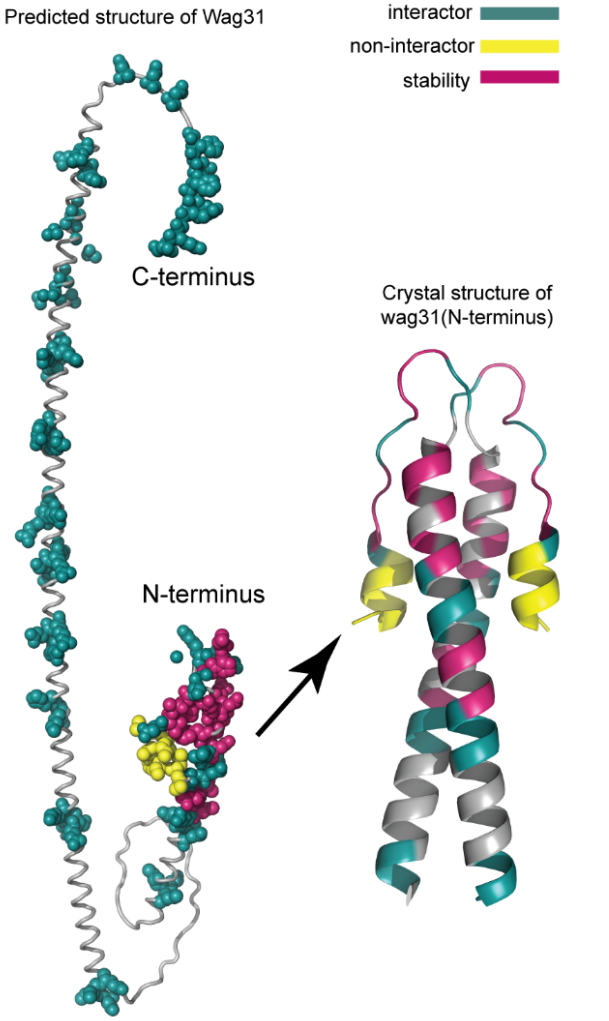

C. Stability of Wag31-DHFR3 fusions by western blot, quantification

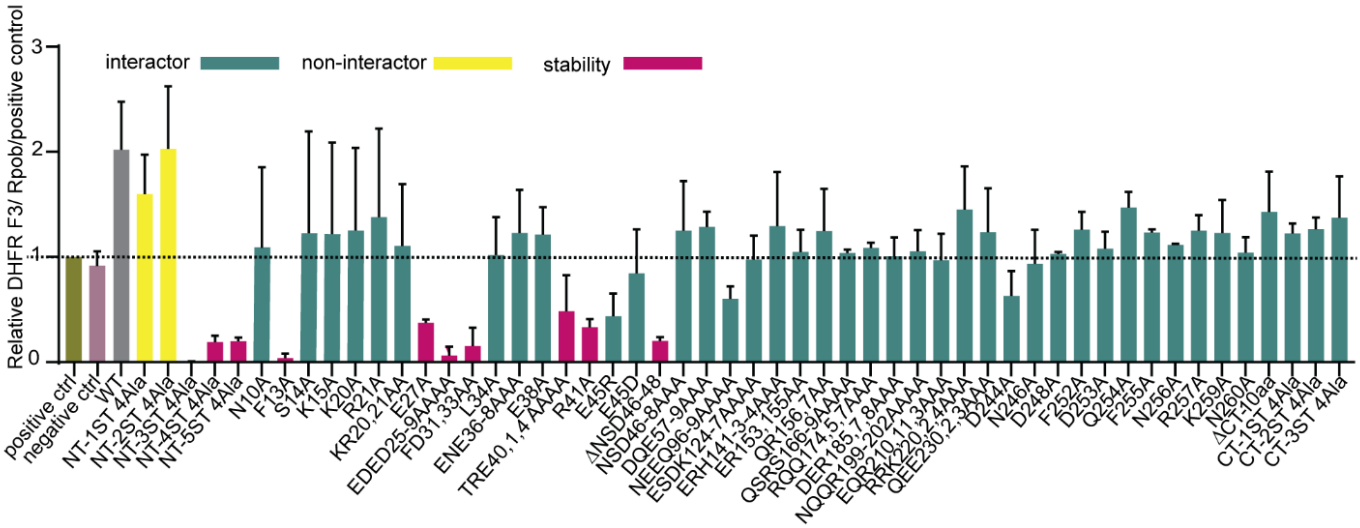

676

677 **Figure 1. Wag31 has multiple sites of interaction of homo-oligomerization.** (A)
678 Representative plates from the Mycobacterial Protein Fragment Complementation two-
679 hybrid assay. Indicated strains were struck out on plates with and without trimethoprim
680 (+TMP/ -TMP). (B) Representative western blots of WT and mutants of Wag31-DHFR3.
681 RpoB serves as a loading control. (C) Normalized quantification of western blot (as in
682 B) band intensities: ratio of ((Wag31-allele/ matched RpoB)/(Wag31 WT/ matched
683 RpoB))/(DHFR-GCN4/ matched RpoB). Values are the mean of western blots from two
684 independent cultures. Error bars represent SD. The dotted line shows the protein level
685 of the DHFR positive control. (D) Alphafold2 predicted structure (Jumper *et al.*, 2021) of
686 a Wag31 monomer (left) and crystal structure of a dimer of the N-terminal 60 amino
687 acids of Wag31 (right) (Choukate and Chaudhuri, 2020). The residues are colored
688 according to the results of the two-hybrid assay and the western blots. Teal: mutants of
689 this residue were stable, but failed to interact with WT Wag31 in the two-hybrid. Pink:
690 mutants of this residue were not stable. Yellow: mutants of this residue were stable, and
691 still interacted with Wag31 in the two-hybrid.

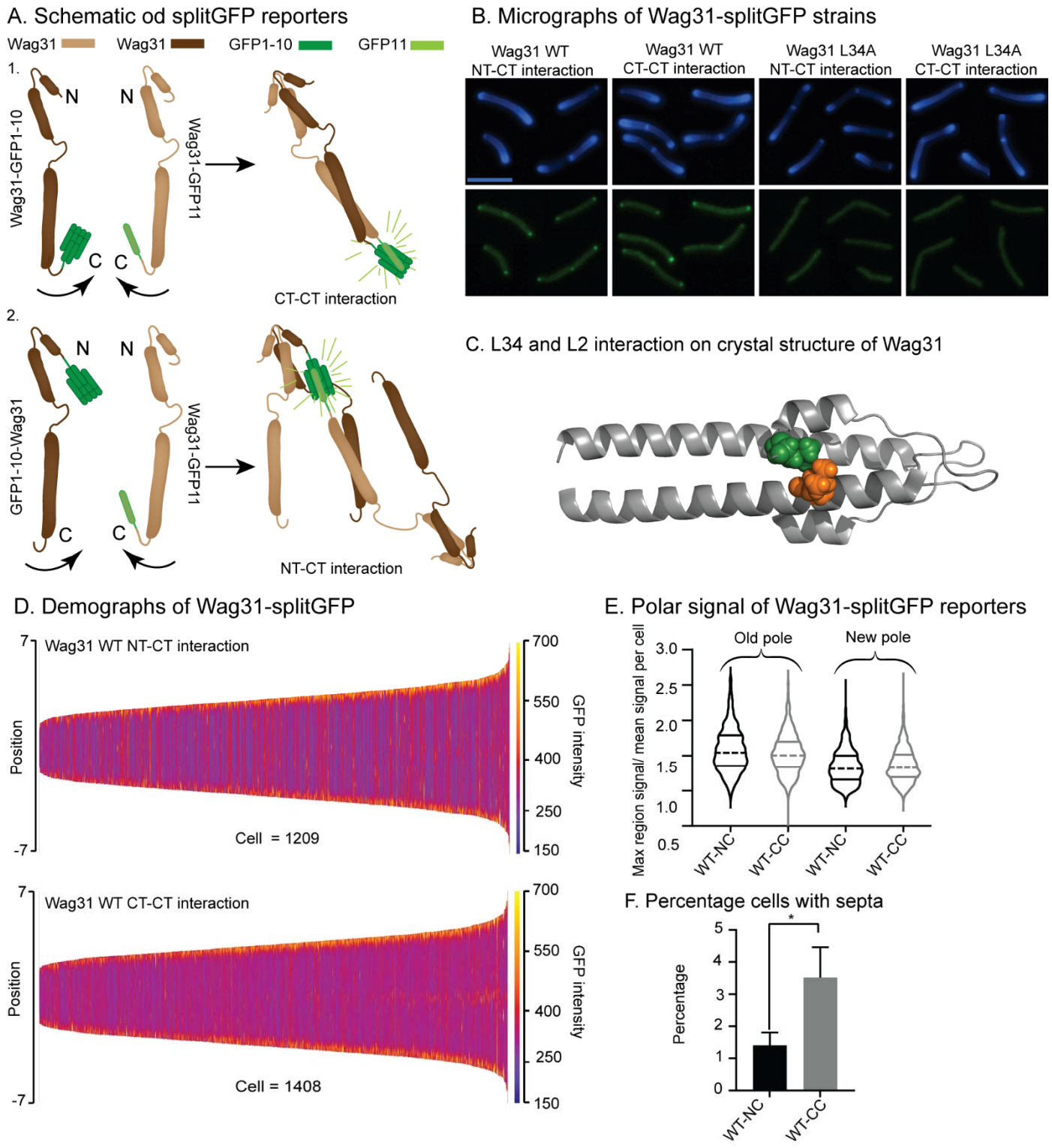

692

693 **Figure 2. Wag31 homo-oligomeric interaction topology is different at the poles**

694 **and septum, and L34 is important for initial interactions.** (A) Schematic of splitGFP

695 reporter strains. Schematic of control strains can be found in supplemental figure (Fig.
696 S8A). (B) Images of *Msmeg* cells expressing Wag31 WT NT-CT interaction reporter,
697 Wag31 WT CT-CT interaction reporter, Wag31 L34A NT-CT interaction reporter, and
698 Wag31 L34A CT-CT interaction reporter. Top: HADA fluorescence; bottom: splitGFP
699 fluorescence. The scale bar is 5 microns, and applies to all images. (C) Hydrophobic
700 interaction between the L2 of one monomer (green) and L34A (orange) another
701 monomer in the dimer crystal structure of the N-terminus of Wag31. (D) Demographs of
702 splitGFP signal intensity across the length of the cell of the WT splitGFP strains of three
703 biological replicates. At least 300 cells were analyzed from each of three independent
704 biological replicates for each reporter. The cells were pole-sorted based on the HADA
705 intensity, with pole 1, the pole that stains more brightly with HADA, at the top. (E)
706 Quantification of splitGFP polar intensity of cells expressing the Wag31 WT NT-CT
707 (black) and CT-CT (gray) splitGFP reporters. (H) Percentage of cells in (E) that have
708 septal splitGFP signal. *, P = <0.05. *P*-values were calculated by the unpaired two-tailed
709 student's *t*-test.

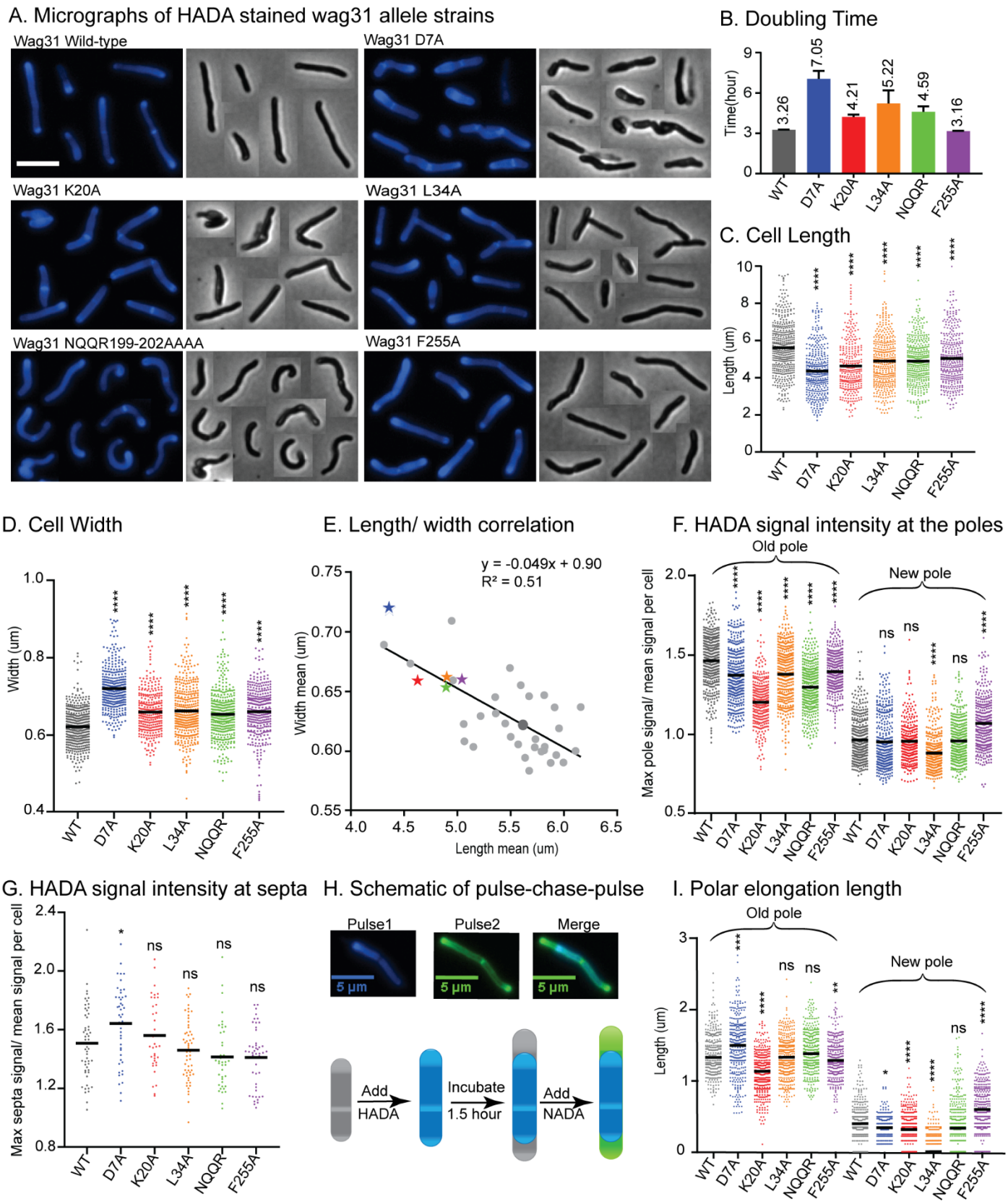
A. Micrographs of HADA stained wag31 allele strains
Wag31 Wild-type
Wag31 D7A
Wag31 K20A
Wag31 L34A
Wag31 NQQR199-202AAAA
Wag31 F255A
B. Doubling Time
Time(hour)
3.26
7.05
4.21
5.22
4.59
3.16
WT
D7A
K20A
L34A
NQQR
F255A
C. Cell Length
Length (um)
D. Cell Width
Width (um)
E. Length/ width correlation
y = -0.049x + 0.90
R² = 0.51
Width mean (um)
Length mean (um)
F. HADA signal intensity at the poles
Old pole
New pole
Max pole signal/ mean signal per cell
G. HADA signal intensity at septa
Max septa signal/ mean signal per cell
H. Schematic of pulse-chase-pulse
Pulse1
Pulse2
Merge
5 µm
Add HADA
Incubate 1.5 hour
Add NADA
I. Polar elongation length
Length (um)

710

Figure 3. Wag31 has multiple distinct roles in both elongation and division. (A) Phase (right) and fluorescence (left) images of *wag31* allele strains stained with HADA. The scale bar is 5 microns, and it applies to all images. (B) Doubling times of *Msmeg* cells expressing WT or *wag31* alanine mutants. The means (on top of bars) are an average of three biological replicates. Error bars represent SD. (C) Cell lengths of the *wag31* allele strains. Black bars are at the mean. (D) Cell widths of the *wag31* allele strains. Black bars are at the mean. (E) Correlation between cell length and cell width. Black bar is linear regression fit. The five mutants in the other panels are shown as colored stars, the rest of mutants are shown as light gray dots, *wag31* WT is a dark gray dot. (F), (G) Relative polar and septal HADA intensity of *wag31* allele strains. (H) Schematic of pulse-chase-pulse staining method. (I) Length of polar elongation in the *wag31* allele strains, as measured by the pulse-chase-pulse method. Black bar is at the median. ns, $p > 0.05$, *, $P = < 0.05$, **, $P =< 0.005$, ***, $P =<0.0005$, ****, $P = <0.0001$. All *P*-values are calculated by one-way ANOVA, Dunnett's multiple comparisons test.

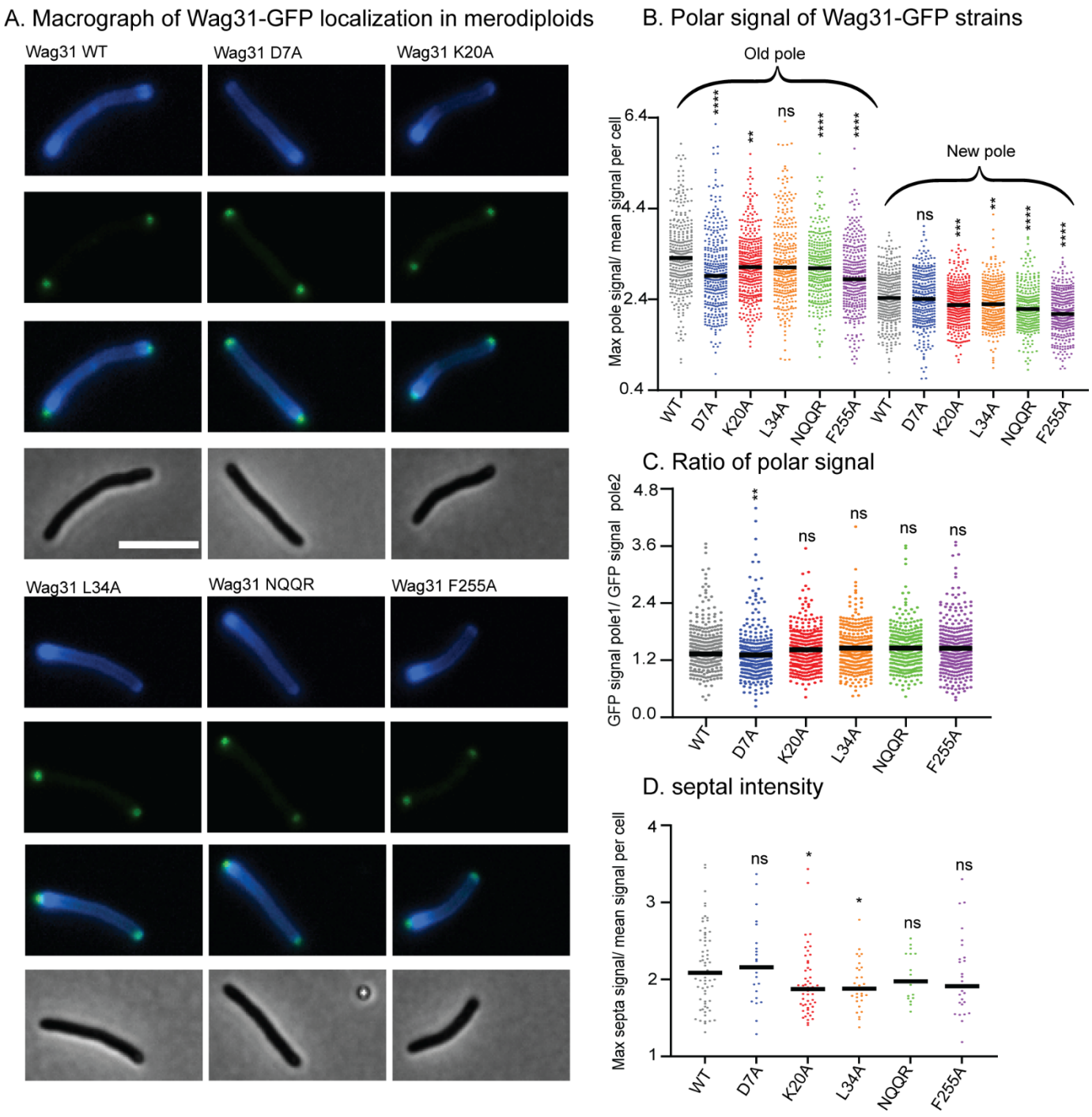

Figure 4. Wag31 mutants localize normally in merodiploid strains. (A) Micrographs of WT *Msmeg* expressing Wag31-GFPmut3 constructs with the indicated mutations. Top: HADA; second: GFP; third: merged; bottom: phase. The scale bar is 5 microns, and it applies to all images. (B) Relative polar intensity of GFPmut3 signal from cells in

731 A. (C) Ratio of normalized signal at the old pole over normalized signal at the new pole,
732 from B. (D) Relative septal intensity of GFPmut3 signal from cells in A. ns, P >0.05, *, P
733 =< 0.05, **, P=< 0.005, ***, P=< 0.0005, ****, P= <0.0001. All *P*-values (B), (C) are
734 calculated by one-way ANOVA, Dunnett's multiple comparisons test and the *P*-value (D)
735 is calculated by the Welch's t-test.
736

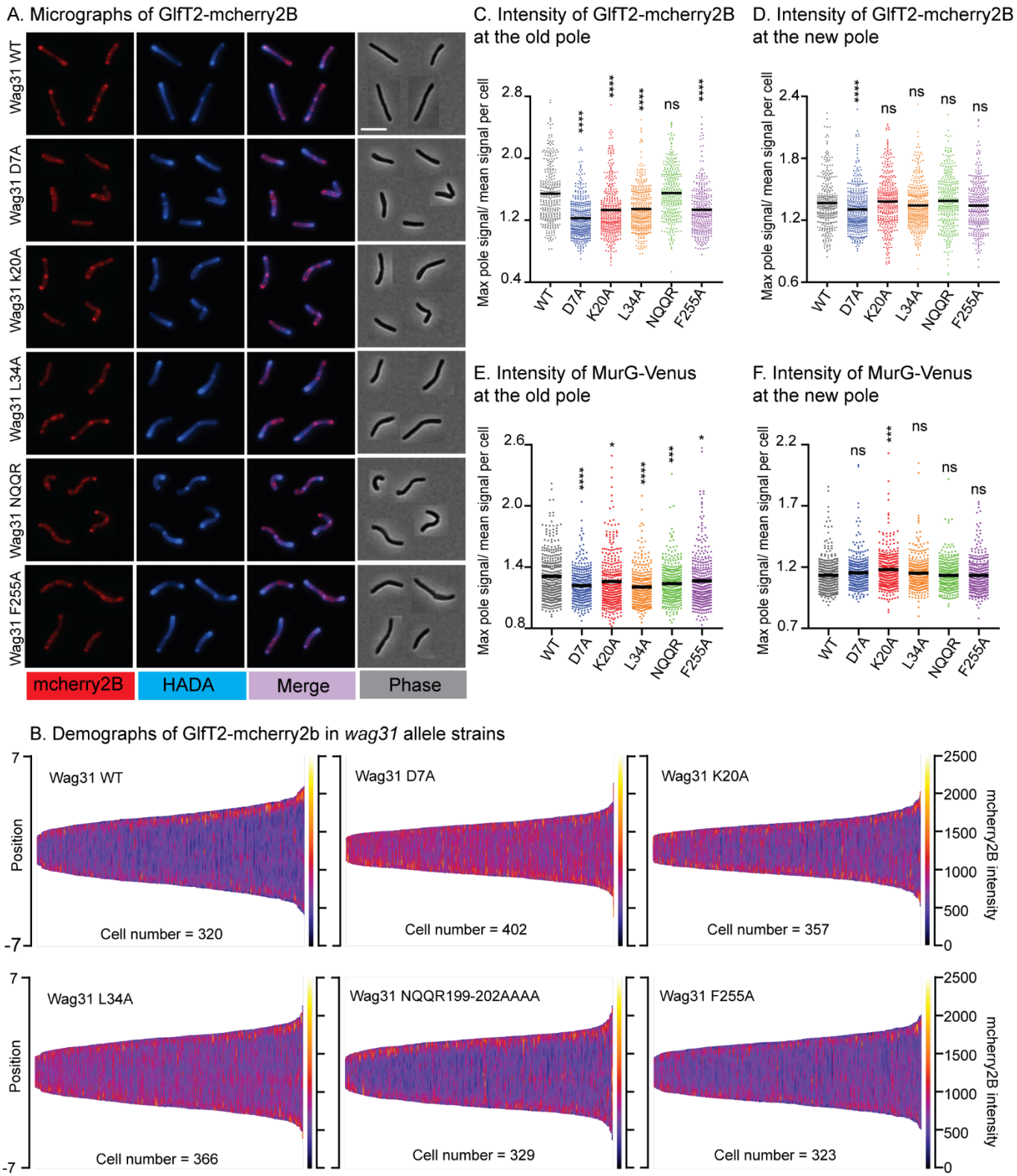
A. Micrographs of GlfT2-mcherry2B
Wag31 WT
Wag31 D7A
Wag31 K20A
Wag31 L34A
Wag31 NQQR
Wag31 F255A
mcherry2B
HADA
Merge
Phase
C. Intensity of GlfT2-mcherry2B at the old pole
D. Intensity of GlfT2-mcherry2B at the new pole
E. Intensity of MurG-Venus at the old pole
F. Intensity of MurG-Venus at the new pole
Max pole signal/ mean signal per cell
WT
D7A
K20A
L34A
NQQR
F255A
ns
B. Demographs of GlfT2-mcherry2b in wag31 allele strains
Wag31 WT
Cell number = 320
Wag31 D7A
Cell number = 402
Wag31 K20A
Cell number = 357
Wag31 L34A
Cell number = 366
Wag31 NQQR199-202AAAA
Cell number = 329
Wag31 F255A
Cell number = 323
Position
mcherry2B intensity

737

738

739 **Figure 5. Localization of IMD proteins does not determine changes in polar**

740 **growth.** (A) Micrographs of *wag31* allele strains expressing GlfT2-mcherry2b and

741 stained with HADA. The scale bar is 5 microns, and it applies to all images. (B)

742 Demographs of GlfT2-mcherry2b intensity across the length of each cell (Y axis of each

743 plot, with intensity indicated by color – scale to the right of each plot), arranged by cell

744 length (along the X axis). At least 100 cells were analyzed for each of three biological

745 replicate cultures. (C) and (D) Polar intensity of GlfT2-mcherry2b at the old pole and the

746 new pole, respectively, from cells in A. (E) and (F) Polar intensity of MurG-Venus at the

747 old pole and the new pole, respectively. ns, P >0.05, ***, P=< 0.0005, ****, P= <0.0001.

748 *P*-value is calculated by one-way ANOVA, Dunnett's multiple comparisons test.

749

750

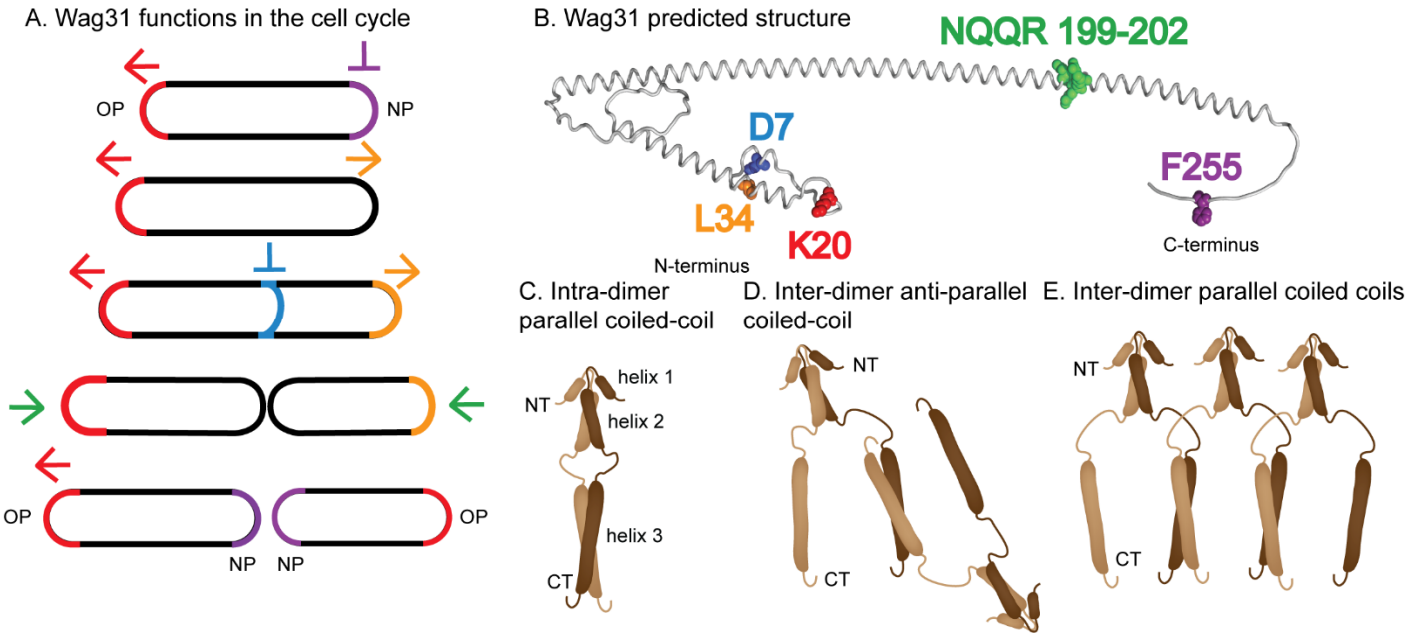

751

752 **Figure 6. Models.** (A) Multiple functions affected by Wag31 are highlighted in different

753 steps of the cell cycle. Red = old pole elongation; purple = inhibition of new pole

754 elongation; orange = new pole elongation; blue = inhibition of septation; green =
755 maintenance of pole structure. (B) The residues shows to affect the functions in (A) are
756 highlighted on an Alphafold2 predicted structure (Jumper *et al.*, 2021) of a Wag31
757 monomer. (C) Model of a Wag31 dimer showing the N-terminal coiled coil of the helices
758 1 and 2 from the crystal structure (Choukate and Chaudhuri, 2020), and a intra-dimer
759 parallel coiled coil of helix 3. (D) Model of a portion of Wag31 network showing an inter-
760 dimer anti-parallel coiled coil of helix 3, with intra-dimer N-terminal interactions as in (C).
761 (E) Model of a portion of Wag31 network showing an inter-dimer parallel coiled coil of
762 helix 3, with intra-dimer N-terminal interactions as in (C).